J Solid State Electrochem (2008) 12:721–728
DOI 10.1007/s10008-007-0415-0

ORIGINAL PAPER

# Corrosion and corrosion inhibition characteristics of bulk nanocrystalline ingot iron in sulphuric acid

**E. E. Oguzie · S.G. Wang · Y. Li · F.H. Wang**

Received: 1 July 2007 / Revised: 5 August 2007 / Accepted: 20 August 2007 / Published online: 19 September 2007


**Abstract** The corrosion and corrosion inhibition of bulk nanocrystalline ingot iron (BNII) fabricated from conventional polycrystalline ingot iron (CPII) by severe rolling was studied in 0.5 M $H_2SO_4$ solution using electrochemical impedance spectroscopy and potentiodynamic polarization techniques. The results indicate that BNII was more susceptible to corrosion in the acidic environment essentially because of an increase in the kinetics of the anodic reaction. An amino acid cysteine (cys) was employed as a corrosion inhibitor at concentrations of 0.001 and 0.005 M. Tests in inhibited solutions revealed that cys reduced the corrosion rates of both metal specimens by different mechanisms. For CPII cys inhibited the cathodic reaction but had a stimulating effect on the anodic process at low concentration and a trivial effect at higher concentration. For BNII, cys inhibited both the cathodic and the anodic reactions, although the former effect was more pronounced. Iodide ions improved the inhibitive effect of cys without altering the inhibition mechanism.

E. E. Oguzie · Y. Li (✉) · F. Wang
State Key Laboratory for Corrosion and Protection,
Institute of Metal Research, Chinese Academy of Sciences,
62 Wencui Road,
Shenyang 110016, China
e-mail: liying@imr.ac.cn

S. Wang
Shenyang National Laboratory for Materials Sciences,
Institute of Metal Research and International Centre
for Materials Physics, Chinese Academy of Sciences,
72 Wenhua Road,
Shenyang 110016, China

E. E. Oguzie
Electrochemistry and Materials Science Research Laboratory,
Department of Chemistry,
Federal University of Technology Owerri,
PMB 1526 Owerri, Nigeria

**Keywords** Iron · Nanocrystallization · Anodic dissolution · EIS · Polarization curves

## Introduction

Iron and its alloys find extensive applications in industry, where they are used in a variety of service environments. In aqueous solutions, the major cause of metallic material degradation and failure is electrochemical corrosion. The corrosion resistance of iron can be considerably upgraded by alloying with other metals as well as reduction in the structural defects and impurity content [1]. These days, nanocrystallization and development of nanocrystalline materials is generating a lot of interest as a means of improving materials performance. Nanocrystalline metals and alloys have been extensively investigated because of the need for better understanding of the nanostructure, vis-à-vis the structural and chemical stability as well as for potential technological applications. A number of studies have examined the corrosion behavior of nanocrystalline materials with contradictory results. Vinogradov et al. [2] found no significant difference in the polarization behavior of ultrafine-grained copper and that of its coarse-grained counterpart. Ye et al. [3] did not observe any noteworthy influence of nanocrystallization on the corrosion behavior of 309 stainless steel in $Na_2SO_4$ solution, whereas a significant improvement in corrosion resistance was observed in NaCl solution. Previous studies in this laboratory revealed that bulk nanocrystalline ingot iron possessed superior corrosion resistance compared to the conventional polycrystalline analogue in HCl as well as 0.05 M $H_2SO_4$+ 0.25 M $Na_2SO_4$ solution [4, 5]. Wang and Li [6] reported that the corrosion resistance of 304 stainless steel in NaCl solution was better than the coarse grained counterpart.

Similar observation was reported for a nanocrystalline surface layer on 316L stainless steel [7] and nanocrystalline zinc coatings [8]. On the other hand, Li et al. reported that the corrosion rate of surface nanocrystallized low carbon steel in acid sulphate solution was higher than that of the bulk steel [9]. In addition, the corrosion resistance of nanocrystalline nickel in sulfuric acid solution was found to be lower than that of the coarse grained nickel [10]. All of the above suggest that the effect of nanocrystallization on corrosion performance is quite sensitive to the nature of the metal system and the environment.

A practical method to protect metallic surfaces deployed in service in aqueous aggressive environments is addition of species to the solution in contact with the surface to inhibit the corrosion reaction and reduce the corrosion rate. The inhibitors hinder the corrosion process by increasing either or both the cathodic and anodic polarization behavior, retarding the transport of ions to the metal/solution interface, or increasing the electrical resistance of the metal surface. Owing to increasing ecological awareness and strict environmental regulations, attention is now focused on the development of substitute nontoxic alternatives, to inorganic inhibitors applied earlier. Amino acids are attractive as corrosion inhibitors because they are nontoxic, relatively easy to produce with high purity at low cost, and are soluble in aqueous media. A number of studies involving amino acids and their derivatives on the corrosion inhibition of iron and its alloys [11, 12], including the corrosion inhibition synergism with other additives [13], can be found in the literature. On the other hand, despite the fact that metal surface conditions and microstructure can influence the efficiency of an applied inhibitor, only little information is available on the corrosion inhibition of their nanocrystalline counterparts. Prior studies in this laboratory revealed that allyl thiourea has a protective effect on conventional polycrystalline ingot iron and an activating effect on the nanocrystalline counterpart in acidic sulfate solution and hydrochloric acid [14, 15]. To extend the investigation to other service conditions, the present study is the first to report on the effect of nanocrystallization on the corrosion and corrosion inhibition of ingot iron in sulfuric acid solution. The test inhibitor chosen for this study is cysteine ($HSCH_2CH[NH_2]CO_2H$; cys), a sulfur-containing amino acid. The influence of iodide ions on the inhibition process was also assessed.

## Experimental section

The test specimens used in this study were a conventional polycrystalline ingot iron (CPII) and bulk nanocrystalline ingot iron (BNII). BNII was prepared from CPII by severe rolling technique. The details of the severe rolling technique and subsequent microstructure characterization of CPII and BNII have been described elsewhere [4]. The specimens were machined into test coupons of dimension 1.2×1.2 cm, which were wet polished with silicon carbide abrasive paper (from grade #400 to #1,000), degreased in acetone, rinsed with distilled water, and dried in warm air.

Electrochemical experiments were performed using an AUTOLAB PGSTAT 30 potentiostat/galvanostat (Eco Chemie BV, The Netherlands) equipped with General Purpose Electrochemical System 4.9 and Frequency Response Analysis 4.9 software. A conventional three-electrode Pyrex glass cell was used for the experiments. Test coupons with exposed surface area 1 $cm^2$ were used as the working electrode and a platinum foil as the counter electrode. The reference electrode was a saturated calomel electrode, which was connected via a Luggin's capillary. The aggressive solution was 0.5 M $H_2SO_4$, prepared from analytical reagent grade concentrated acid using distilled water. Corrosion tests were also carried out in 0.001 and 0.005 mol $dm^{-3}$ solutions of the test inhibitor, cys, prepared by dissolving appropriate amounts of the solid compound in 0.5 M $H_2SO_4$. The influence of iodide ions on the inhibition process was assessed by introducing 0.005 mol $dm^{-3}$ KI into inhibited solutions containing 0.005 M cys. All experiments were undertaken in stagnant aerated solutions at 30±1 °C. The working electrode was immersed in a test solution for 30 min or until a stable open circuit potential was attained (usually about 40 min in the blank acid). Potentiodynamic polarization studies were carried out in the potential range ±250 mV vs corrosion potential ($E_{corr}$) at a scan rate of 0.333 mV $s^{-1}$. Electrochemical impedance spectroscopy (EIS) measurements were made at corrosion potentials ($E_{corr}$) over a frequency range of 10 kHz–10 mHz, with a signal amplitude perturbation of 5 mV. Spectra analyses were performed using Zsimpwin software.

## Results and discussion

### Open-circuit potential measurements

The evolution of the open-circuit potential (OCP) with time for the two iron specimen in 0.5 M $H_2SO_4$ without and with addition of 0.005 M cys are shown in Fig. 1. The OCP variations in the pure acid solution show some distinguishable characteristics. CPII displays an instantaneous shift of potential toward positive (noble) values, which corresponds to the growth of a surface film on the electrode. For BNII, the displacement of OCP toward more positive values is not immediate, rather an initial slight decay of potential to

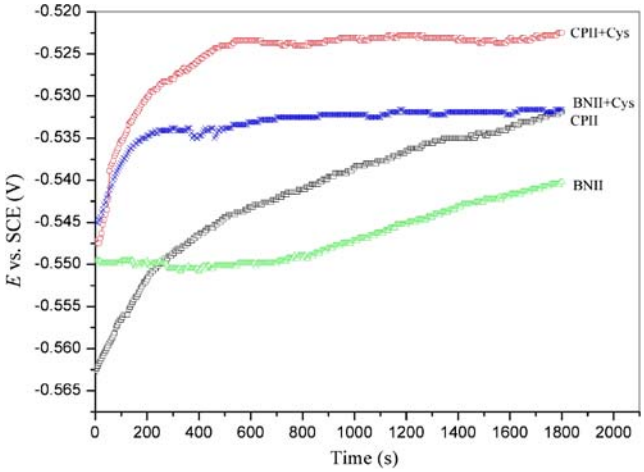


**Fig. 1** Variation of open circuit potential (OCP) with time for CPII and BNII in 0.5 M $H_2SO_4$ without and with 0.005 M cys

negative (active) values is observed for BNII, after which the potential stabilizes for a brief period before shifting toward noble values. In addition, the attained OCP values (at $t$>200 s) were always more positive for CPII.

On introduction of cys into the acid solution, the potential shift and attainment of a stable OCP becomes more rapid and the potentials reach more noble values than those observed in the blank acid for both specimens (about 10–15 mV). This can be attributed to the formation of a protective layer of cys on the electrode surfaces.

## Electrochemical impedance spectroscopy measurements

The key objective of EIS experiments is to provide insight into the characteristics and kinetics of electrochemical processes, which occur at the CPII/0.5 M $H_2SO_4$ and BNII/0.5 M $H_2SO_4$ interfaces. The impedance response of these systems is presented in Fig. 2a,b,c, which exemplify, respectively, the Nyquist, Bode, and phase angle plots. It is obvious that nanocrystallization resulted in a decrease in the size of the semicircle in Fig. 2a, in the impedance of the interface in Fig. 2b, and in the maximum phase angle in Fig. 2c, indicating a decline in the corrosion resistance. The impedance plots for CPII and BNII after 2 h of immersion are presented in Fig. 3. Compared to the results in Fig. 2a, the impedance and hence corrosion resistance of both samples increased with time. This can be attributed to the slow adsorption of reaction products at dissolution sites and a consequent decrease in corrosion rate [16]. The Nyquist plots for all systems generally have the form of only one depressed semicircle, which corresponds to one time constant in the Bode plots. The single time constant may be attributed to the short exposure time in the corrodent, which is insufficient to reveal degradation of the substrate. The depression of the Nyquist semicircle with the center under the real axis is typical for solid metal electrodes that

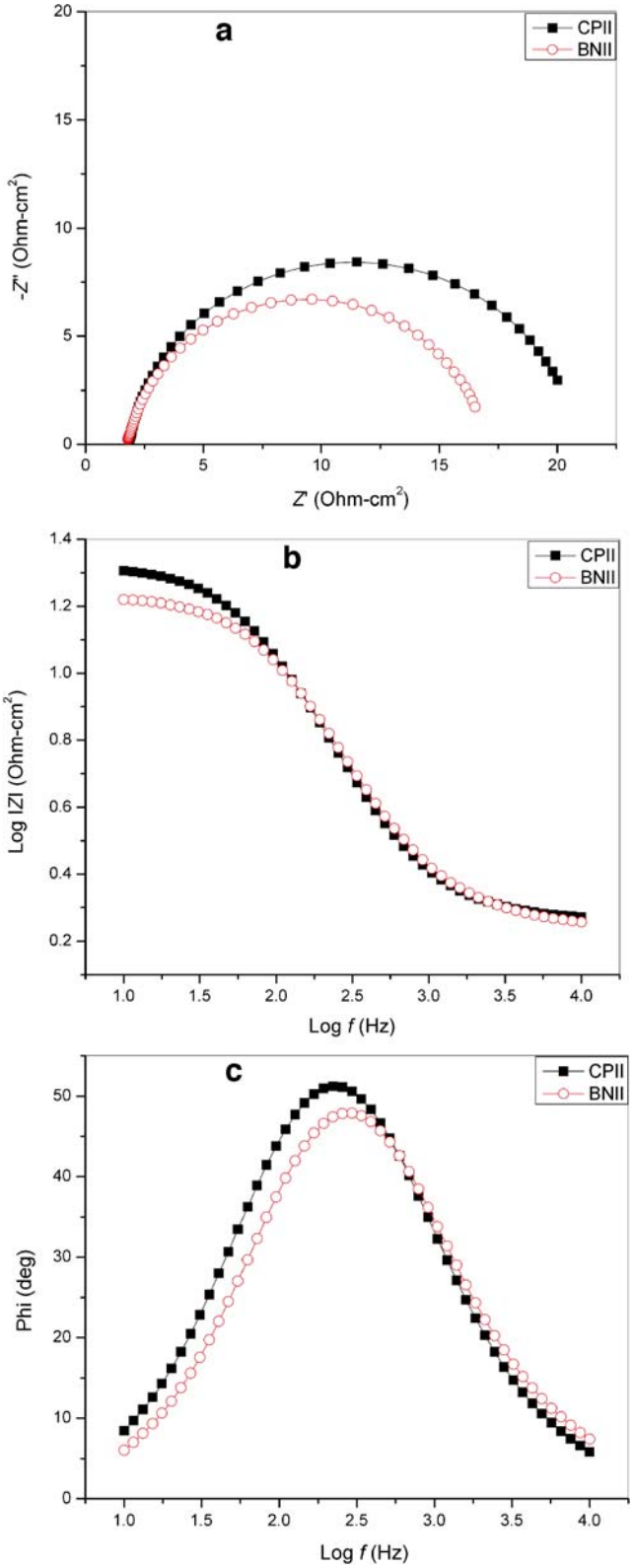


**Fig. 2** Electrochemical impedance plots of CPII and BNII in 0.5 M $H_2SO_4$ without inhibitor after 30 min immersion; **a** Nyquist, **b** Bode, and **c** phase angle plots

show frequency dispersion of the impedance data. The transfer function can be represented by a solution resistance

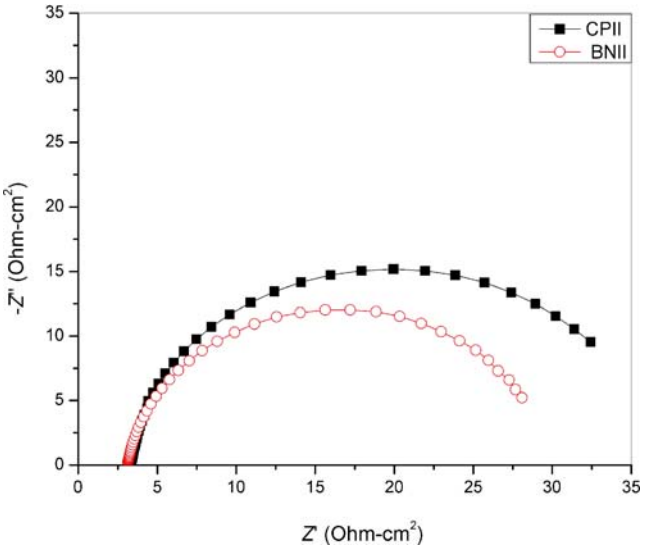


**Fig. 3** EIS Nyquist plots of CPII and BNII in 0.5 M $H_2SO_4$ without inhibitor after 2 h immersion

$R_s$, shorted by a capacitor ($C$) that is placed in parallel to the charge transfer resistance $R_{ct}$ [17]:

$$Z_{(\omega)} = R_s + \left(\frac{1}{R_{ct}} + j\omega C\right)^{-1} \quad (1)$$

This transfer function is, however, only applicable for homogeneous systems with one time constant when the center of the semicircle lies on the abscissa and cannot account for the depression of the capacitive semicircle. When a nonideal frequency response is present, the capacitor is replaced by a constant phase element (CPE). The use of such a CPE has been extensively described in the literature [17, 18]. The impedance, $Z$ of the CPE is:

$$Z_{CPE} = Q^{-1}(j\omega)^{-n} \quad (2)$$

where $Q$ and $n$ stand for the CPE constant and exponent, respectively, $j=(-1)^{1/2}$ is an imaginary number, $\omega$ is the angular frequency in rad $s^{-1}$, ($\omega=2\pi f$) when $f$ is the frequency in hertz. The parameter $n$ is generally accepted to be a measure of surface inhomogeneity.

The impedance spectra for the Nyquist plots were appropriately analyzed by fitting to the equivalent circuit model $R_s(Q_{dl}R_{ct})$, which has been previously used to model the Fe/acid interface [17–19]. The corresponding electrochemical parameters are given in Table 1. It can be seen that the charge transfer resistance of BNII (15.1 Ω $cm^2$) is lower than that of CPII (19 Ω $cm^2$), indicating a higher corrosion susceptibility of the former. The proportionality factor $Q$ of CPE does not show significant variation for the two samples. $Q$ values are associated with the surface area available for the cathodic reaction [19]. In addition, $n$ values are about the same, probably because for the short immersion periods the density of the corrosion products was low.

**Table 1** Impedance parameters for CPII and BNII in 0.5 M $H_2SO_4$

| System | $R_{ct}$ (Ω $cm^2$) | $Q$ (μΩ$^{-1}$ $s^n$ $cm^{-2}\times10^{-4}$) | Number |
|---|---|---|---|
| CPII | | | |
| Blank (0.5 h) | 19.0 | 2.08 | 0.92 |
| Blank (2 h) | 33.2 | 2.07 | 0.94 |
| BNII | | | |
| Blank (0.5 h) | 15.1 | 1.98 | 0.92 |
| Blank (2 h) | 26.6 | 1.70 | 0.94 |

Experiments were also undertaken to assess the influence of the microstructure of ingot iron on the efficiency of a corrosion inhibitor (0.005 M cys). The impedance spectra of CPII and BNII in 0.5 M $H_2SO_4$ solution containing 0.005 M cys are given in Fig. 4 and shows that the impedance responses of both metal specimens do not differ significantly. The Nyquist plots again correspond to a single depressed semicircle as observed in the blank acid, and as such, the same equivalent circuit was thus used to fit the experimental data. Compared to Fig. 2, an increase in the impedance parameters of both CPII and BNII can be seen in the presence of cys, which is associated with the corrosion-inhibiting effect of the additive. $R_{ct}$ values increased to 29.7 and 27.5 Ω-$cm^2$ for CPII and BNII, respectively, while the corresponding values of the proportionality factor $Q$ of CPE reduced to 159 and 149 μΩ$^{-1}$ $s^n$ $cm^{-2}$. Such decrease in $Q$ values normally results from a decrease in the dielectric constant and an increase in the double layer thickness, which suggests that cys molecules are adsorbed on the metal/electrolyte interface [17, 18]. This can be rationalized by considering the Helmholtz model; $C_{dl} = \varepsilon\varepsilon_o A/\delta$, where $\varepsilon$ is the dielectric constant of the medium, $\varepsilon_o$ the vacuum permittivity, $A$ the electrode area, and $\delta$ the thickness of the protective layer. The smaller dielectric constant of the organic molecule compared to water as well as the increase in the thickness of the double layer because of cys adsorption act to reduce the interfacial capacitance. Inhibition efficiency was calculated from $\left[\eta_R\% = \left(1 - R_{ct}/R'_{ct}\right) \times 100\right]$, where $R_{ct}$ and $R'_{ct}$ are the values of the charge transfer resistance in absence and presence of cys. The obtained values were 36% for CPII and 45% for BNII, which indicates that the nanocrystalline microstructure of BNII provides a more favorable surface for cys adsorption in the 0.5 M $H_2SO_4$ solution.

## Polarization measurements

Polarization experiments were particularly undertaken to distinguish the effect of nanocrystallization on the anodic and cathodic corrosion reactions of ingot iron in sulfuric acid. Typical anodic and cathodic polarization curves of CPII and BNII in the 0.5 M $H_2SO_4$ solution are illustrated

in Fig. 5, and the corresponding electrochemical parameters given in Table 2. Both samples exhibit active dissolution without any distinctive transition to passivation within the studied potential range. It is, however, obvious that bulk nanocrystallization led to an increase in the kinetics of the anodic metal dissolution, whereas the cathodic process was not markedly affected. The value of the corrosion potential ($E_{corr}$) was also slightly lowered from −523 mV for CPII to −534 mV in the case of BNII, while the corrosion current ($i_{corr}$) increased from 628 to 841 μA cm$^{-2}$. This is again indicative of a higher corrosion susceptibility of BNII.

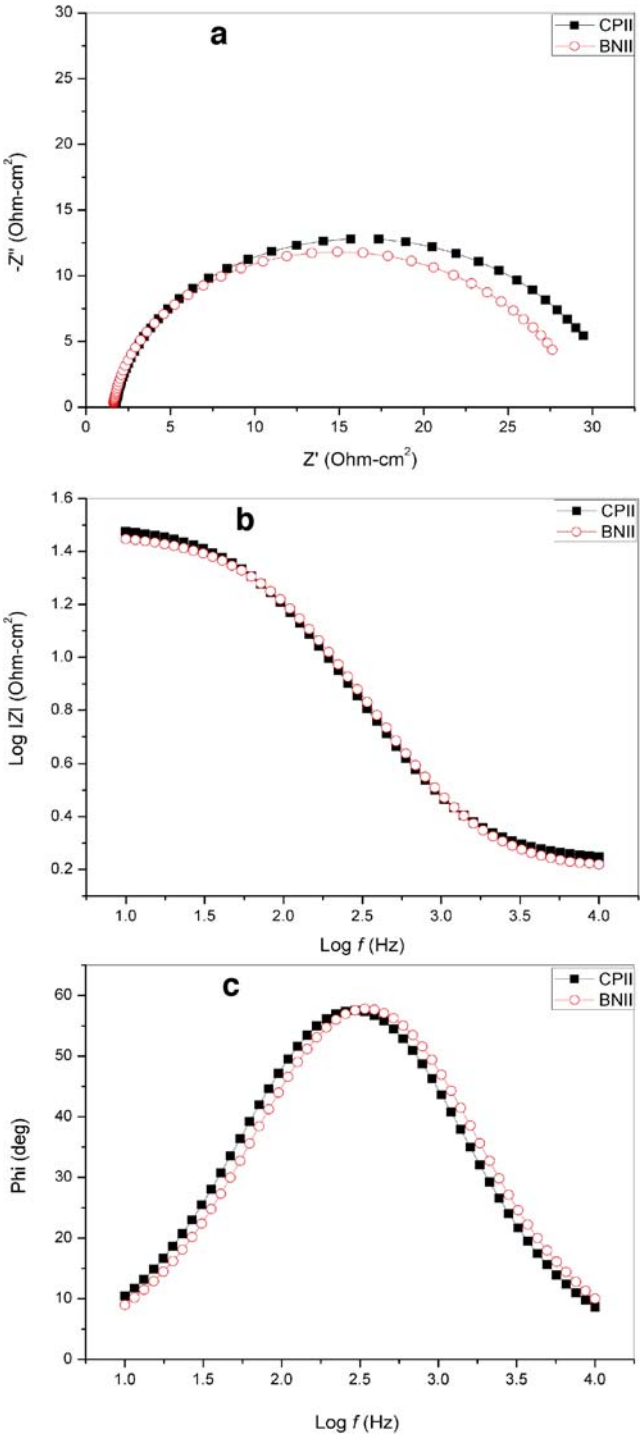


**Fig. 4** Electrochemical impedance plots of CPII and BNII in 0.5 M $H_2SO_4$ solution containing 0.005 M cys after 30 min immersion; **a** Nyquist, **b** Bode, and **c** phase angle plots

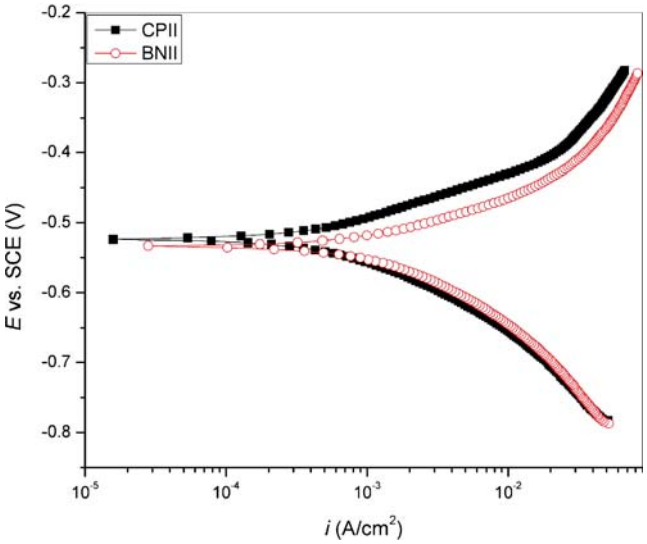


**Fig. 5** Polarization curves of CPII and BNII in 0.5 M $H_2SO_4$ without inhibitor

Microstructure characterization revealed identical composition for CPII and BNII[4], and considering the Fe anodic dissolution reaction $\left(Fe_{(s)} \rightarrow Fe^{2+}_{(aq)} + 2e\right)$, it can be rightly implied that the discrepancy in their corrosion behavior is mainly due to the differences in grain size and the subsequent structural modification. BNII with mean grain size 38.9 nm (compared to 50 μm for CPII) provides a greater surface area as well as a high population of active sites, which could accelerate the kinetics of the anodic reaction (Eq. 3) by forming several microelectrochemical corrosion cells. In addition, the considerable volume of grain boundaries, which for passive metals and alloys is

**Table 2** Polarization data for CPII and BNII in 0.5 M $H_2SO_4$ with cys

| System | $E_{corr}$ (mV) | $i_{corr}$ (μA cm$^{-2}$) | $\beta_c$ (mV dec$^{-1}$) | $B_a$ (mV dec$^{-1}$) |
|---|---|---|---|---|
| CPII | | | | |
| Blank | −523 | 628 | 109 | 77 |
| 1 mM cys | −524 | 1022 | 166 | 68 |
| 5 mM cys | −509 | 559 | 153 | 59 |
| Cys+5 mM KI | −521 | 190 | 114 | 58 |
| BNII | | | | |
| Blank | −534 | 841 | 125 | 76 |
| 1 mM cys | −522 | 717 | 160 | 62 |
| 5 mM cys | −516 | 483 | 151 | 53 |
| Cys+5 mM KI | −532 | 215 | 133 | 56 |

often advantageous for outward diffusion of film-forming elements, in the present case serve as fast diffusion conduits for the corrosive medium. All of these could contribute to the higher dissolution kinetics of BNII compared to CPII.

A number of mechanistic studies on the anodic dissolution of Fe in aqueous solutions have been undertaken, and the hydroxyl-accelerated mechanism proposed initially by Bockris et al. [20] and Heusler [21] has gained overwhelming acceptance. The mechanism postulates the initial formation of the adsorbed intermediate $(FeOH)_{ads}$. According Heusler, the dissolution mechanism corresponds to:

$$Fe + (FeOH)_{ads} \rightarrow Fe(FeOH)_{ads} \quad (3)$$

$$Fe(FeOH)_{ads} + OH^- \rightarrow FeOH^+ + (FeOH)_{ads} + 2e \quad (4)$$

$$FeOH^+ + H^+ \rightarrow Fe^{2+} + H_2O \quad (5)$$

Equations 4 and 5 represent the slow stage and the rapid stage, respectively. Reduction in the number of defects has been shown to shift the equilibrium of Eq. 3 to the left [1], which corresponds to an overall reduction in the Fe dissolution rate. Intercrystaline constituents, grain boundaries, and triple junctions are considered to be distinct defects that provide active dissolution sites [5]. The increase in their population as a result of nanocrystallization can thus be correlated to increased population of defects in BNII. The higher dissolution kinetics of BNII could then be related to a shift of the equilibrium of Eq. 5 to the right. Rofagha et al. [22] are also of the opinion that the increased volume fraction of grain boundaries and triple junctions account for the higher dissolution kinetics of nanocrystalline Ni–P compared to its polycrystalline counterpart in 0.1 M $H_2SO_4$. The enhanced corrosion rate of BNII in 0.5 M $H_2SO_4$ could also be attributed to the presence of high stored energy and residual stress as well as extensive plastic deformation resulting from the severe rolling process [23]. The effects of plastic deformation are generated by an increase in the number and activity of surface sites, and subsequent corrosion acceleration for iron is due essentially to an increase in the rate of the anodic dissolution reaction, as the cathodic hydrogen evolution reaction is not significantly affected by plastic deformation [4, 5]. This in fact corroborates our findings in the present study (Fig. 5), where severe rolling led to an increase in the kinetics of the anodic dissolution of ingot iron in the sulfuric acid solution, whereas the cathodic reaction was scarcely affected.

It is obvious that the results of the present study in the 0.5 M $H_2SO_4$ solution, vis-à-vis the higher corrosion susceptibility of BNII compared to CPII, is opposed to the results from an earlier study in 0.05 M $H_2SO_4$+0.25 M $Na_2SO_4$ solution, where BNII exhibited a much higher corrosion resistance than CPII [5]. Several factors could be responsible for this observation, including the very corrosive nature of the sulfuric acid solution, which mitigates the formation of a protective passive layer on BNII. This is another demonstration of the wide-ranging variation in the corrosion performance and properties of nanocrystalline materials in different environments.

Polarization experiments were also undertaken to determine the effect of cys on the anodic and cathodic reactions of CPII and BNII. The polarization curves obtained for both specimens in 0.5 M $H_2SO_4$ containing 0.001 and 0.005 M cys are illustrated in Fig. 6, and the electrochemical parameters also given in Table 2. $E_{corr}$ values were only slightly shifted by addition of cys, while the Tafel region in the cathodic branch of the polarization curves becomes wider in the presence of cys. For CPII (Fig. 6a), cys is observed to

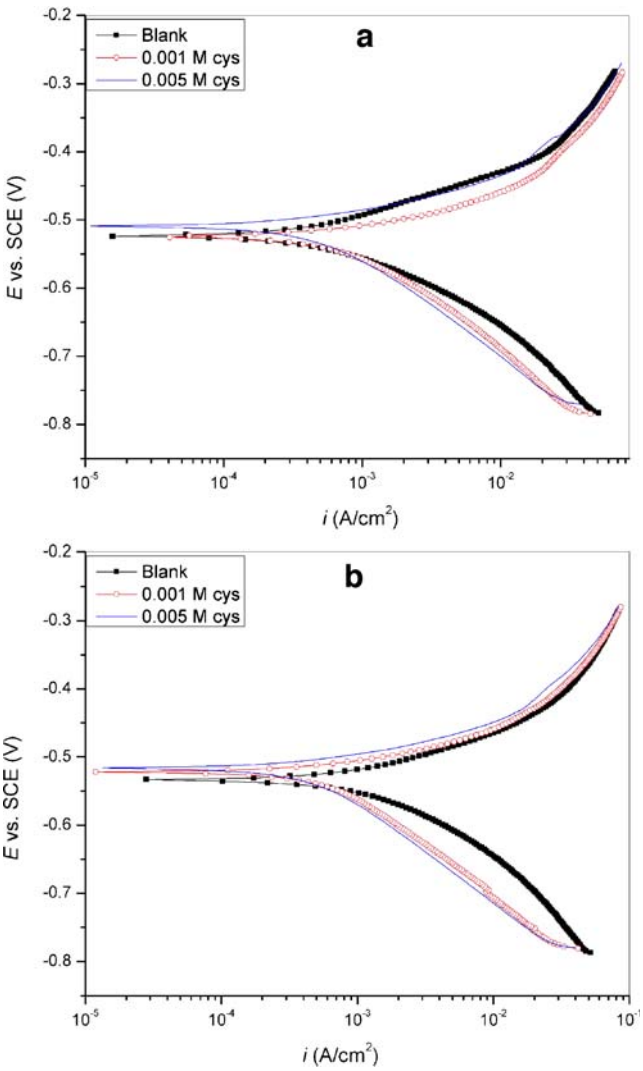


**Fig. 6** Polarization curves of **a** CPII and **b** BNII in 0.5 M $H_2SO_4$ containing 0.001 and 0.005 M cys

exert an inhibiting effect on the cathodic reaction at both concentrations but had insignificant effect on the anodic reaction at higher concentration (0.005 M) and an activating effect at lower concentration. Thus cys functioned essentially as a cathodic inhibitor for CPII at the studied concentrations. For BNII (Fig. 6b), cys is again seen to significantly inhibit the cathodic reaction, but in this case, the anodic reaction is inhibited as well, although to a lesser extent. Thus, cys herein functioned as a mixed-type inhibitor, with a predominant cathodic action. The anodic-inhibiting effect, which was not observed for CPII, may suggest that the higher anodic reaction kinetics of BNII in 0.5 M $H_2SO_4$ with the increased number of active corrosion sites probably becomes beneficial for inhibitor adsorption. This is because the population of active adsorption sites also increases correspondingly, which effect would reduce the adsorption equilibrium period. Inhibition efficiency was calculated from the polarization data by $\left[\eta_1\% = \left(1 - i'_{\mathrm{corr}}/i_{\mathrm{corr}}\right) \times 100\right]$, where $i'_{\mathrm{corr}}$ and $i_{\mathrm{corr}}$ are the corrosion current densities in the presence and absence of cys. The calculated values show that cys, at a lower concentration, stimulated the corrosion of CPII ($\eta\%$=−61%) at 0.001 M concentration but had a protective effect ($\eta\%$=11%) at 0.005 M. On the other hand, $\eta\%$ values for BNII were 15 and 43% at [cys]=0.001 and 0.005 M, respectively. Although the $\eta\%$ values obtained from polarization experiments are somewhat different from those from the EIS technique, both show the same trend. Lower values from the polarization data implies predominant influence of the anodic dissolution process is in determining the corrosion rate. The fact that cys exerted a greater inhibiting effect on BNII is again in contrast to earlier findings [14, 15]. This disparity could be attributed to difference in the nature of the corrosive media and the applied inhibitors. Moreover, BNII exhibited superior corrosion resistance in other environments, and as pointed out by Oblonsky et al. [24], the more stable passive film could prevent optimal inhibitor adsorption.

The polarization curves obtained for CPII and BNII in the presence of 0.005 M KI added to 0.5 M $H_2SO_4$ inhibited by 0.005 M cys are presented in Fig. 7. The plots obtained in the presence of cys alone have been included for comparison. The introduction of iodide ions is seen to further improve the ability of cys in inhibiting the corrosion reaction. Consequently, protection efficiency attained values of 69.7 and 74.4%, respectively, for CPII and BNII. The mechanism of this synergistic effect has been described in detail in earlier reports [25–27]. Briefly, the iodide ions, which are strongly chemisorbed on the corroding metal surface, facilitate cys adsorption by acting as intermediate bridges between the positively charged metal surface and cys cations, formed by protonation of the cys molecule in the acid solution. This stabilizes the adsorption of cys on the metal surface, leading to higher surface coverage. Figure 7 clearly shows that the iodide ion effect did not alter the inhibition mechanism of cys on both CPII and BNII.

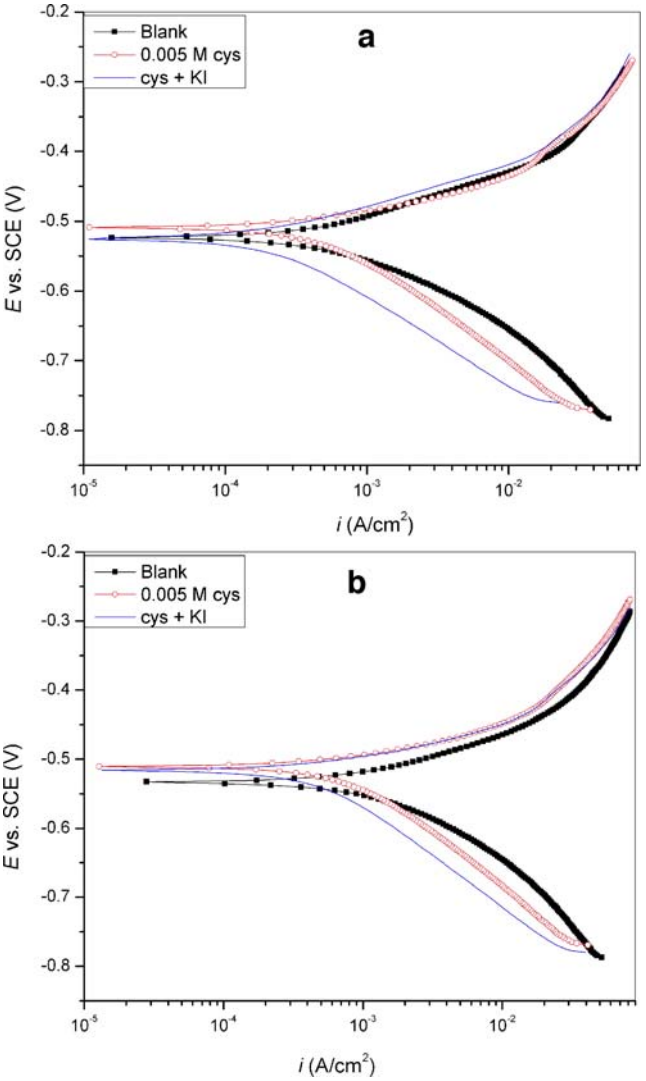


**Fig. 7** Polarization curves of **a** CPII and **b** BNII in 0.5 M $H_2SO_4$ containing 0.005 M cys and 0.005 M KI+0.005 M cys

## Conclusions

Bulk nanocrystallization effected by severe rolling technique diminished the corrosion resistance of ingot iron in the 0.5 M $H_2SO_4$ solution by accelerating the kinetics of the anodic metal dissolution process. Cys functioned as a corrosion inhibitor for both the polycrystalline (CPII) and the nanocrystalline (BNII) iron samples, exerting a greater inhibiting effect on the latter. The inhibition mechanism was affected by the microstructure of the sample. For CPII, cys functioned strictly as a cathodic inhibitor, whereas for BNII, both the cathodic and the anodic reactions were inhibited in the presence of cys. Although iodide ions

increased the protective efficiency of cys, the inhibition mechanism remained unaffected.

**Acknowledgments** E.E. Oguzie is grateful to the Chinese Academy of Sciences (CAS) and the Academy of Sciences for the Developing World (TWAS) for the award of CAS-TWAS Fellowship. Financial support from the National Natural Science Foundation of China under contract no. 50501023 is gratefully acknowledged.

## References

1. Bala H (1984) Electrochim Acta 29:119
2. Vinogradov A, Mimaki T, Hashimoto S, Valier RZ (1999) Scripta Mater 41:319
3. Ye W, Li Y, Wang FH (2006) Electrochim Acta 51:4426
4. Wang SG, Shen CB, Long K, Yang HY, Wang FH, Zhang ZD (2005) J Phys Chem B 109:2499
5. Wang SG, Shen CB, Long K, Zhang T, Wang FH, Zhang ZD (2006) J Phys Chem B 110:377
6. Wang XY, Li DY (2002) Electrochim Acta 47:3939
7. Kwok CT, Cheng FT, Man HC, Ding WH (2006) Mater Lett 60:2419
8. Youssef KhMS, Koch CC, Fedkiw PS (2004) Corros Sci 46:51
9. Li Y, Wang F, Liu G (2004) Corrosion 60:891
10. Mishra R, Balasubramaniam R (2004) Corros Sci 46:3019
11. Moretti G, Guidi F, Grion G (2004) Corros Sci 46:387
12. Silva AB, Agostinho SML, Barcia OE, Cordeiro GGO, D'Elia E (2006) Corros Sci 48:3668
13. Morad MS, El-Hagag A, Hermas A, Abdel Aal MS (2002) J Chem Technol Biotechnol 77:486
14. Shen CB, Wang SG, Yang HY, Long K, Wang FH (2006) Electrochim Acta 52:3950
15. Shen CB, Wang SG, Yang HY, Long K, Wang FH (2006) Appl Surf Sci 253:2118
16. Muralidharan VS, Rajagopalan KS (1979) Corr Sci 19:199
17. Popova A, Christov M (2006) Corr Sci 48:3208
18. Sayed SY, El-Deab MS, El-Anadouli BE, Ateya BG (2003) J Phys Chem B 107:5575
19. Lopez DA, Simison SN, de Sanchez SR (2003) Electrochim Acta 48:845
20. Bockris JO'M, Drazic D, Despic AR (1961) Electrochim Acta 4:325
21. Heusler KE (1958) Z Electrochem 62:582
22. Rofagha R, Langer R, El-Sherik AM, Erb U, Palumbo G, Aust KT (1991) Scripta Metall Mater 25:2867
23. Evans UR (1960) Corrosion and oxidation of metals. Edward Arnold, London
24. Oblonsky LJ, Chesnut GR, Devine TM (1995) Corrosion 51:891
25. Oguzie EE (2005) Mater Chem Phys 87:212
26. Oguzie EE, Onuoha GN, Onuchukwu AI (2004) Mater Chem Phys 89:305
27. Oguzie EE, Li Y, Wang FH (2007) J Coll Interf Sci 310:90